Applied Spectroscopy
XX(X):1–9

DOI: 10.1177/ToBeAssigned
www.sagepub.com/

Spatially resolved lateral transmission measurements to characterize changes in the scattering coefficient and the anisotropy factor

Sabrina Stocker[1], Florian Foschum[1], and Alwin Kienle[1]

Abstract

A new setup is described to characterize the scattering coefficient and the scattering phase function of liquid media. The setup utilizes the basic idea of a spatially resolved reflectance measurement combined with a sophisticated illumination geometry. The sample is illuminated parallel and close to the interface of the sample and a glass window to get information from single scattered and multiple scattered light. By illuminating the sample with a fiber orientated with the axis parallel to the glass surface, small distances to the source can be examined unimpeded by the illumination beam. The derived information is for example not only sensitive to the concentration of the scatterers but also to the size of the scattering particles. We present the setup including the theory to describe the light propagation in the whole configuration by Monte Carlo simulations. The validation has been done with polystyrene microsphere dispersions with different scattering coefficients. As application for the developed setup we show measurements of different milk samples which vary in concentration of fat, protein and in fat droplet size during homogenization process. By measuring milk, we show the ability of the sensor to determine information about the scattering phase function without diluting the sample. For sensors in the dairy industry a measurement with no pre-processing and no diluting of the sample is worthwhile, because this can be used to determine the fat and protein concentration on-line.

Keywords

lateral transmission measurement, spatially resolved transmission, scattering phase function, Monte Carlo simulation, milk, anisotropy factor, scattering coefficient

Introduction

Over the past years it has been shown that it is useful to characterize turbid media by separating the scattering and the absorption properties of a sample. This is e.g. important to describe the light propagation in different media properly. There are many methods to determine the (reduced) scattering coefficient $\mu_s(')$ and the absorption coefficient μ_a by e.g. measuring the spatially resolved reflectance[1,2,3], the total reflectance[4,5], detecting the reflected and transmitted light with an integrating sphere[6,7,8], detecting reflected light in the time domain[9,10], detecting the reflected light during illumination of the sample in the spatial frequency domain[11,12,13] or with photon density wave spectroscopy[14]. The radiative transfer theory (radiative transfer equation, RTE)[15] can be used to describe the light propagation in scattering media and hence determine the reduced scattering and the absorption coefficient. To get information about the scattering phase function of the particles, goniometric measurements[16] can be performed on samples with low scattering coefficients. There are already approaches for lateral measurements, but in the setup described in Berrocal et al.[17] also low scattering coefficients are needed. Vaudelle et al.[18] describes calculations for layered media, but no measurements are presented.

The goal of this work was the design of a setup which helps detecting information from the scattering phase function and the scattering coefficient of highly scattering liquid samples. The need of such a setup emerged e.g. in measuring and characterizing milk samples[19]. For fat emulsions like milk, a dilution of the sample changes the concentration

[1]Institut für Lasertechnologien in der Medizin und Meßtechnik, Helmholtzstr. 12, D-89081 Ulm, Germany

Corresponding author:
Sabrina Stocker
Email: sabrina.stocker@ilm-ulm.de

of the emulsifier and hence can change the stability of the emulsion, like the droplet size including the scattering behavior[20,21,22,23]. To determine the optical properties of milk properly, the certain way is to measure milk undiluted which is the advantage of the presented setup. Since the fat droplet size and the fat concentration affect the scattering behavior in milk, it is necessary to separate both influences.
In this work, we present a setup to measure the lateral transmission spatially resolved including the theoretical description of the light propagation in the setup by Monte Carlo (MC) simulations. The MC simulations were then used to examine the influence of the reduced scattering coefficient μ_s', the absorption coefficient μ_a, the anisotropy factor g and the scattering phase function on the detected 2D intensity pattern. Here, two exemplary wavelengths were chosen. First, $405\,\mathrm{nm}$ as a wavelength in the blue and second, $635\,\mathrm{nm}$ in the red wavelength range, because we expect a different behavior for these wavelengths for small particles around hundreds of nanometer in diameter compared to larger particles having a diameter of a few micrometers. To get more spectroscopic information, the wavelengths could be varied systematically through the whole UV/VIS wavelength range. Furthermore, in the result section, measurements of polystyrene (PS) microsphere dispersions with different PS concentrations and hence with different reduced scattering coefficients μ_s' are presented to validate the setup. At the end of the result section, different milk measurements are shown. The milk samples vary in fat concentration, protein concentration and in fat droplet size. The changes in the detected signal arising by changing the individual parameters are presented.

Experimental setup

In order to investigate the light propagation close to the source a sample container with a glass window was designed. A cuvette was printed using black acrylonitrile butadiene styrene (ABS), which is a thermoplastic polymer often used for 3D prints. In Fig. 1, a schematic of the setup with the cuvette is shown. A CCD camera (QSI 640, Quantum Scientific Imaging, Mississippi, US) was used in combination with a lens and a pinhole capturing the transmitted light through a cover slip fixed in the cuvette with a thickness of $150\,\mu\mathrm{m}$. A blue laser diode with $405\,\mathrm{nm}$ and a red laser diode with $635\,\mathrm{nm}$ (both TOPAG Lasertechnik GmbH, Germany) were used as light sources, which were connected to the sample cuvette through an optical fiber with $105\,\mu\mathrm{m}$ core diameter and 0.10 numerical aperture. The fiber was attached to the cuvette in a drilled hole about $250\,\mu\mathrm{m}$ below the surface of the window by an epoxy resin adhesive, so the sample is illuminated from the side and the transmitted light is detected perpendicular through the glass window. In the figure, a generic simulation of the light is depicted on the glass surface where the light emerges the sample.

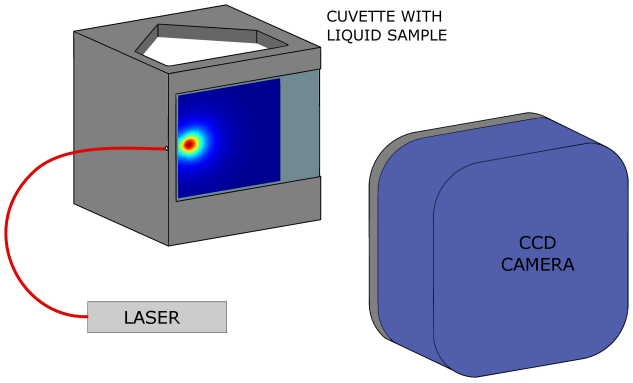

Figure 1. Schematic of the experimental setup with the 3D printed cuvette with a glass window where a generic simulation indicates the measured intensity profile.

Materials and Methods

Materials

Polystyrene microspheres For validation measurements, commercially available polystyrene microspheres were used (Microparticles GmbH, Berlin, Germany). The particles were dispersed in water. The dispersions were prepared in three different concentrations and measured by the lateral transmission setup as well as by an integrating sphere setup and a collimated transmission setup to determine the scattering coefficient and the reduced scattering coefficient. The results of the last two methods were used to control the scattering behavior and to verify Mie theory calculations which were necessary to get the scattering phase function for the MC simulations. For the Mie calculations, the refractive index of the particles was taken from the literature[24] and the size of the particles was given by the manufacturer ($d_{\mathrm{mean}} = 4.43\ \mu\mathrm{m}$). The refractive index was multiplied by a factor of 1.0001 to describe the μ_s and μ_s' measurements properly. A log-normal distribution for the particle size was assumed in the way that the scattering cross section was calculated for some grid points of the distribution and then summarized to the total scattering coefficient. The concentrations of the particle dispersion was chosen such that the reduced scattering coefficient was about $1\,\mathrm{mm}^{-1}$, $2\,\mathrm{mm}^{-1}$ and $3\,\mathrm{mm}^{-1}$ at the wavelength of $600\,\mathrm{nm}$. Further about $2\,\mu\mathrm{L}$ sodium dodecyl sulfate (SDS) solution was given to the sample to make sure no agglomeration or other surface effects are changing the scattering behavior. Before each

measurement the sample had been put in an ultrasonic bath for about 30 min.

Milk samples Different milk samples were used to check the usability of the newly developed setup. Three main milk sorts were used: skim milk, heavy cream and raw milk. They were mixed in different ways to reach different fat and protein concentrations. The size of the fat droplets was changed by homogenization of the raw milk. The sample preparation and the homogenization process was performed as already described in an earlier publication [19].

Monte Carlo simulations

For the MC simulations, the scattering phase functions and the scattering coefficients μ_s were calculated by Mie theory and controlled with measurements with an integrating sphere setup. The light source was simulated as an optical fiber with a core diameter of 105 µm and a numerical aperture of 0.10. The illumination fiber was attached to the volume perpendicular to the yz plane in positive x direction. The detector was orientated perpendicular to the incident beam and detects the photons which leave the sample volume in negative z direction through the xy plane. A schematic of the geometry and a simulated path is shown in Fig. 2. At

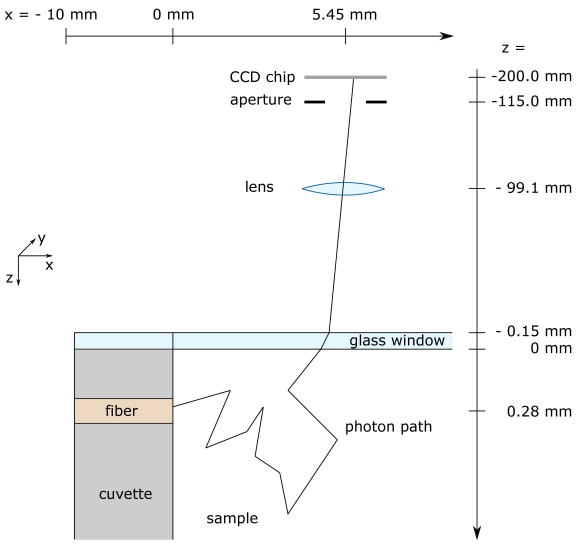

Figure 2. Schematic drawing of the simulated geometry of the setup. As light source an optical fiber embedded in the black cuvette material is shown. The detection of the photons take place through a lens and an aperture. A generic photon path is illustrated propagating through the sample and exiting the sample volume through a glass window in direction of the detector. The exact position of the photon reaching the CCD chip is registered to create a 2D image of the intensity pattern.

the surface of the scattering volume a thin glass window (d =150 µm) was located. Without this glass window a meniscus to the border in the yz plane would disturb the surface. For the glass layer the refractive index was given by the manufacturer to be $n = 1.5255$. Also a low scattering and low absorption coefficient was assumed as $\mu_s' = 0.0001$ mm^{-1} and $\mu_a = 0.0001$ mm^{-1} as well as a Henyey-Greenstein (HG) scattering phase function [25] with an anisotropy factor $g = 0.6$, since the scattering is low the value of the anisotropy factor will carry no weight. The optical properties of the cuvette were assumed to be $n = 1.48$, $\mu_s' = 1$ mm^{-1}, $\mu_a = 1$ mm^{-1} and also with a HG scattering phase function with $g = 0.6$. These values were assumed to be similar to the optical properties of black epoxy resin, which is often used as optical phantom and well investigated in our group [26]. The optical fiber was located 280 µm below the glass layer. In the simulations, the transmitted light through the glass window was detected spatially resolved by a CCD chip through a system of a lens ($f = 50$ mm, Position $z = -99.1$ mm) and an aperture ($d = 8.3$ mm, Position $z = -115$ mm) which images the glass-sample-interface. The distance between the glass window and the CCD chip was 200 mm. With the real detector geometry only a small part of simulated photons reach the detector. Hence, it was necessary to find a method to get a good statistics without changing any geometry. A variance reduction method was implemented since a different detector geometry (like detecting all transmitted photons) would falsify the result, because the aperture of the camera also influences the shape of the 2D pattern. Therefore a method called ”last flight estimation” was used [27,28,29].

We found a deviation of the measurements compared to the simulations for the PS samples with different scattering coefficients. It turned out that this deviation can be explained by changing the fiber diameter of the illumination. For the presented simulations a fiber diameter of 200 µm has been used instead of 105 µm. This parameter affects mainly the intensity profile at small distances to the illumination. Since the bare fiber was glued into a drilled hole using epoxy resin, this larger diameter can be explained by light coupling into the glue. Consequently, a larger effective fiber diameter illuminates the sample.

Results

Pre-calculations for changing scattering phase function

To check the sensivity of the detected signal to changes in the scattering phase function, we simulated the intensity profile for several media with different types of scattering phase

functions $p(\vartheta)$ and alternating anisotropy factors

$$g = \frac{\int_0^\pi p(\vartheta)\ \cos\vartheta\ \sin\vartheta\ d\vartheta}{\int_0^\pi p(\vartheta)\ \sin\vartheta\ d\vartheta} \quad (1)$$

with ϑ as scattering angle. We assumed two different samples with two types of scatterers, milk fat and casein micelles. For each type the scattering phase function was calculated by Mie theory. For milk fat, a size of $3.5\,\mu\mathrm{m}$ was assumed for the mean diameter of the particles and a log-normal distribtion with a width of 0.16. These sizes correspond to the size of fat particles in raw milk[19]. For casein micelles, a mean diameter of $200\,\mathrm{nm}$ was assumed with a width of 0.15 for the log-normal distribution. The calculated scattering phase functions result in anisotropy factors of 0.97 for milk fat and 0.63 for casein micelles. To compare them with other scattering phase functions, the simulations have also been done with an HG scattering phase function for the same anisotropy factors of $g = 0.97$ and $g = 0.63$. The reduced scattering coefficient had been fixed to $3\,\mathrm{mm}^{-1}$ and the absorption coefficient to $0.001\,\mathrm{mm}^{-1}$ for all simulations. In Fig. 3, the intensity along the center line, which is the line along the extended fiber axis, is plotted against the distance to the edge of the cuvette for all four simulations. The

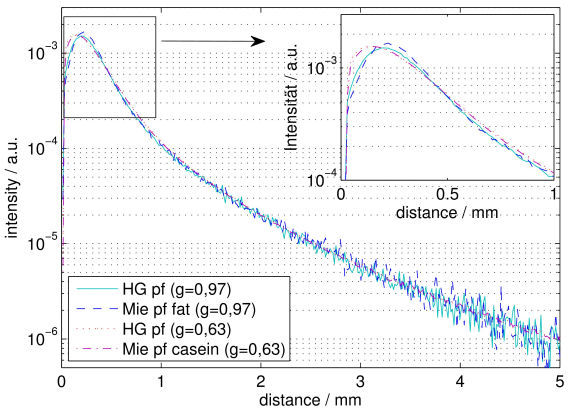

Figure 3. Simulated intensity profile along the center line of the intensity pattern for different samples. The intensity is plotted against the distance to the illumination point. Two simulations with a Mie theory scattering phase function (dashed and dash-dotted line) and two with HG phase function (solid and dotted line). The reduced scattering coefficient of each simulated sample was taken as $3\,\mathrm{mm}^{-1}$ and the absorption coefficient as $0.001\,\mathrm{mm}^{-1}$. The anisotropy factors of the samples were 0.97 (solid and dashed line) and 0.63 (dotted and dash-dotted line). In the inset in signal for small distances is shown in detail.

different scattering phase functions as well as the varying anisotropy factor does not change the slope of the curve for large distances, but the signal for small distances. Regarding small distances, an increase of the anisotropy factor results in a shift of the intensity peak to larger distances for both scattering phase functions. For the smaller anisotropy factor $g = 0.63$, the difference between the two types of scattering phase functions is smaller than for $g = 0.97$. The HG phase function deviates from the Mie theory phase function for small scattering angles, especially for large anisotropy factor like $g = 0.97$, which explains the larger deviations of the signal for an higher anisotropy factor. Hence, a change in the anisotropy factor as well as in the scattering phase function can be detected with this setup. Another approach would be the examination of the influence of the phase function parameter γ or higher moments. For example, the γ values for the presented HG scattering phase functions with $g = 0.63$ and $g = 0.97$ are $\gamma = 1.63$ and $\gamma = 1.97$, respectively. As a higher moment the σ parameter introduced by Bodenschatz et al.[30] can be used. The values are $\sigma = 0.9860$ and $\sigma = 1.1019$ for the HG scattering phase functions with $g = 0.63$ and $g = 0.97$, respectively. For a further examination the different scattering phase function types should be simulated with a constant γ or σ. Such examinations were already published in the spatial domain and the spatial frequency domain[30].

PS dispersion

To validate the setup, three different concentrations of PS dispersions were measured. The samples were measured successively with the lateral transmission setup using both illumination wavelengths. The results of the measurements were compared to MC simulations. The comparison of the 2D images as contour plots are shown in Fig. 4. Here, the intensity is plotted logarithmically, so each iso-intensity line correspond to 0.2 orders of magnitude. The contour plots show that the measured intensity profile for different scattering coefficients is described well by the MC simulations. The intensity pattern gets more ovally shaped for lower concentrations and hence lower scattering coefficients. The same behavior is described in the simulation. To have a closer look on the patterns, the center line of the measured 2D image was calculated. Therefore, the intensity pattern was divided into the even and odd part. These parts can be calculated for each point along the x-axis. The center line was positioned at the x-value for which the odd part is zero, which gives the position with the highest symmetrical part. Then the intensity along the center line is plotted versus the distance to the illumination point. To get better statistics we plotted the mean value of 9 pixel columns around the center line. For better comparability the intensity was normalized to the maximum of the curve. In Fig. 5, the intensity curves for the lowest concentration

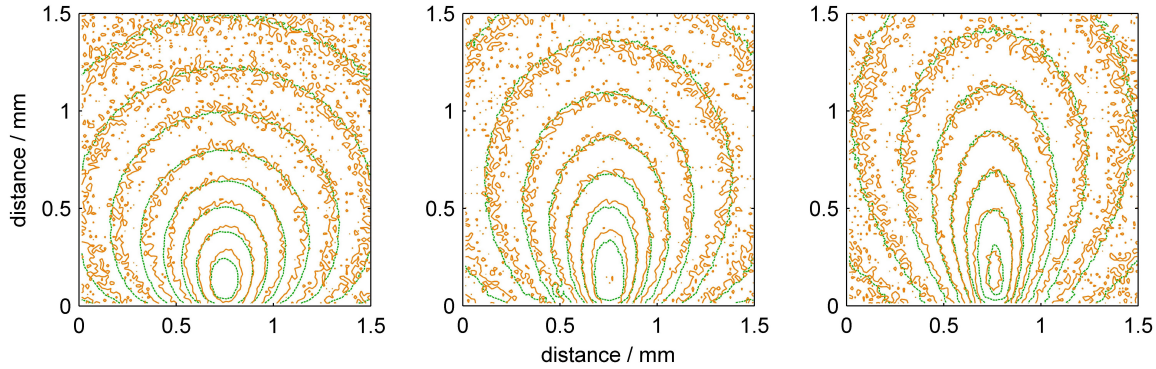

Figure 4. Comparison of 2D intensity images as contour plots for three different samples with decreasing concentration from left to right. The measurements are shown in green color (dashed lines) and the simulations to each measurement in orange color (solid lines).

with two different illumination wavelengths are shown exemplarily. In the upper and lower part of the figure the

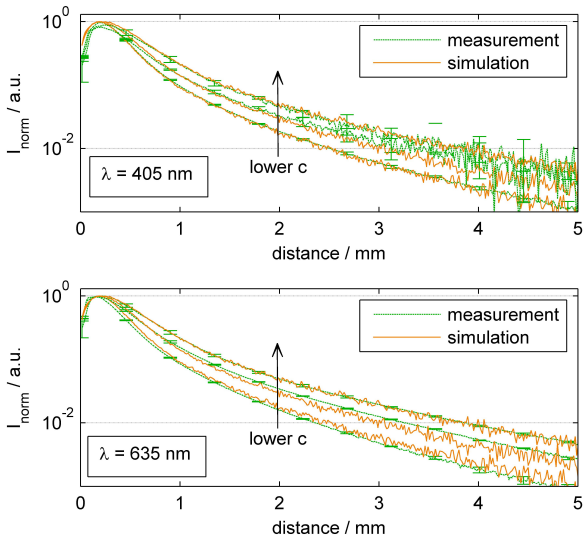

Figure 5. Normalized intensity curvature along the center line of the 2D image as a logarithmic plot against the distance to the illumination. In the upper part the measurement is compared to the simulation for the $405\,\mathrm{nm}$ illumination, in the lower part for the $635\,\mathrm{nm}$ illumination. The error bars give the standard deviation of three repetitions with refilled samples in between the measurements. The measurements are shown in green color (dashed lines) and the simulations to each measurement in orange color (solid lines).

intensity for the $405\,\mathrm{nm}$ and $635\,\mathrm{nm}$ illumination is given, respectively. The error bars represent the standard deviation of three measurements of the same sample. In between these measurements, the cuvette was removed from the setup and the sample was refilled. The measurements show a good reproducibility. In the case of the $405\,\mathrm{nm}$ illumination, we get less signal for larger distances compared to the $635\,\mathrm{nm}$ illumination. In both cases, the width of the intensity peak and the slope during the decrease are well described by the simulations.

Milk samples

A possible application field for such a setup is the characterization of milk. In case of raw milk, the fat particle sizes vary for each cow and during the milking process [19] and so the scattering behavior can change with constant fat or protein content. An advantage of the presented setup is that information of the particle size can be measured without diluting the sample. As a first proof of principles we measured different milk samples with varying fat and protein contents and varying particles sizes.

In order to test the sensors's sensitivity to fat and protein concentration, we mixed homogenized skim milk and homogenized heavy cream. In combination with water we produced a sample pattern with different fat and protein contents. The fat content varied between $1\,\%$ to $5\,\%$ and the protein content between $2\,\%$ to $4\,\%$. The raw data of the 2D images ($635\,\mathrm{nm}$ illumination) detected with the CCD camera are shown in Fig. 6 on the left in logarithmic scale. To get a better idea of the impact for varying fat and protein content, we calculated the relative deviation of the intensity to the sample with mid-fat content and mid-protein content. These images are shown in Fig. 6 on the right side. It can clearly be seen that a change in fat content dominates the shape of the image. This can be found along the vertical line of the shown grid. The contour of the intensity profile gets more roundish for a higher fat content. The effect of changing protein can hardly be seen even in the relative images. The intensity along the center axis is plotted versus the distance to the fiber again averaged over the 9 middle columns. The results are shown in Fig. 7. The strong dependence on the fat content can also be seen in this depiction, especially for the small distances. However, for larger distance a dependency on the protein content can be found as well. A change of about $1\,\%$ in protein content does not change the intensity maximum in

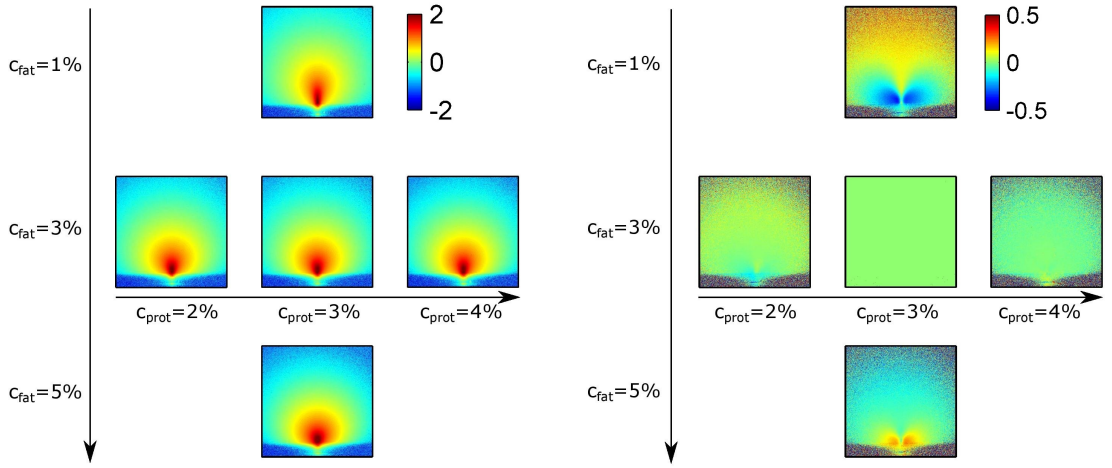

Figure 6. 2D images of the remitted light of the lateral transmission setup for five different milk samples with varying fat and protein content. In the left part of the figure the raw intensity data is shown in logarithmic scaling. In the horizontal line the protein content is changing and in the vertical line the fat content is. In the right part the change in the images is emphasized by taking the signal relative to the sample with the mid-fat concentration and mid-protein concentration (sample in the center of the pattern).

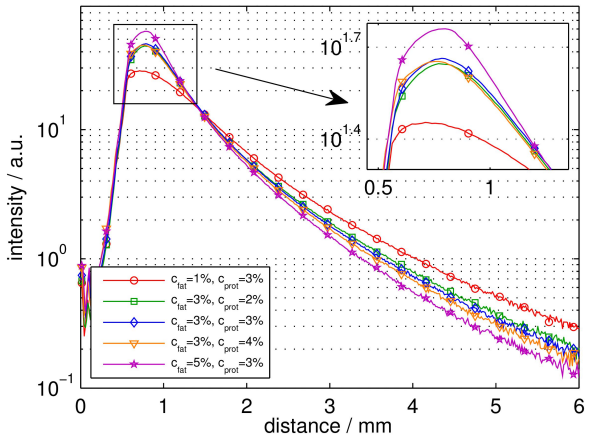

Figure 7. Intensity along the center line of the 2D images (635 nm illumination) averaged over 9 colums around the center line plotted versus the distance to the illumination position. For the plots red, blue and purple (circles, diamonds and stars) the protein content was constant. For the colors green, blue and orange (squares, diamonds and triangles) the fat content was constant.

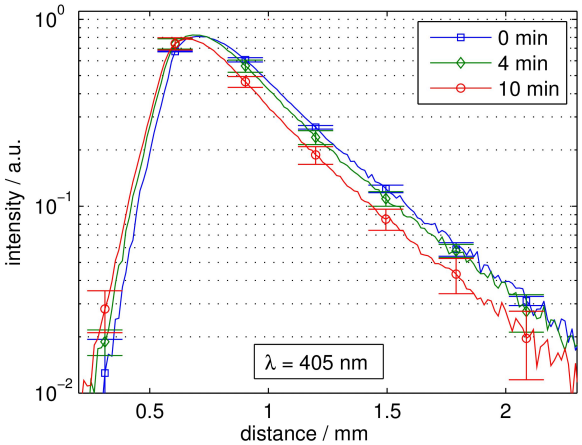

Figure 8. Intensity along the center line of the 2D images (405 nm illumination) for three raw milk samples after different homogenization steps. The intensity is plotted versus the distance to the illumination position. The homogenization degree is increase from the blue curve (squares) over the green curve (diamonds) to the red curve (circles) and hence the droplet size was lowered for these samples.

a systematic way, but for larger distances a systematic change can be seen.

To examine the influence of fat droplet size, milk samples were produced with fresh raw milk. Two samples of the raw milk were then homogenized for 4 min and 10 min. For better lucidity we refrain from showing all 2D images of the measured samples. In the case of changing droplet sizes, we want to highlight the effect during homogenization for the illumination with 405 nm. In Fig. 8, the intensity along the center line as described in preceding sections is plotted. The change in particle size droplet affects the width of the intensity peak on the whole distance range. These results show that varying fat droplet size result in a different signal with the presented setup. Since the absolute value of the maximum is not influenced, varying fat droplet sizes should be separable from varying fat concentrations. However, a change in droplet size with constant volume concentration results in a different reduced scattering coefficient as well. So not only the scattering phase function is affected as assumed in the simulations presented in the 'pre-calculations' section, but also the scattering coefficient.

Conclusion

In this work, a new setup for the examination of scattering liquid samples had been described. In the setup the sample was illuminated laterally with two wavelengths in small

distance and parallel to a surface which was imaged by the CCD chip of a camera. The light propagation in the setup was calculated by MC simulations which are numerical exact solutions of the radiative transfer equation. The simulations showed that the detected signal is sensitive to the scattering phase function also for highly scattering and undiluted samples. The setup was verified by polystyrene microspheres and then applied to different milk samples.

By applying the MC simulations, the exact geometry could be considered. These simulations showed that the setup is sensitive to changes in the scattering phase function. By comparing measurements and simulations of PS microsphere samples we could show that the theory describes the light propagation in the setup well. The simulations describe not only the intensity decrease along the incident beam axis but also the 2D intensity pattern which was imaged by the CCD camera for three samples with different scattering coefficients. To give an application for such a setup, different milk samples were analyzed. Milk is a medium in which the fat droplet size changes for each cow, for instance, and hence the scattering phase function, but also the scattering coefficient for different concentrations of the scatterers varies. The used milk samples varied in fat concentration, protein concentration and fat droplet size. Each variation produced a different detected intensity pattern. An important result is that a change in fat droplet size affects the intensity decrease in a different way as a change in fat concentration. This is important since a separation of these parameters can help measuring the fat concentration of raw milk without any dilution or pre-treatment necessary. In the last years, milk has often been measured by different diffuse reflectance measurements[31,32,33,34,35] partly the idea of an oblique illumination has already been applied[36]. Our setup differs from these measurements since it is more sensitive to changes in the scattering phase function and the anisotropy factor. The advantage of the lateral transmission setup over the oblique incident reflectometry is the independence over surface roughness. A possible approach to determine the optical properties of milk quantitatively would be the training of a neural network. Therefore, by simulating a large set of milk samples, the relevant areas of the intensity patterns characterizing the fat and protein contents should be determined. Another advantage of the use of a neural network would be the fast analysis once the network is trained. Another approach is the determination by chemometrical methods like already reported in literature[37,38]. For more spectroscopic information, the illumination wavelengths could be varied systematically over a larger wavelength range. With further simulations and examinations of the optical properties of milk, the idea of this setup can be helpful to create a calibration free method to determine the fat and protein content in milk during the whole milk production process. Also for other liquid samples, especially emulsions, this setup can be useful to get information about the scattering phase function. Especially, because due to measurement at the side of the sample, the method is less prone to error by surface roughness compared to measurements on top of the sample. In the case of goniometric measurements low values of the scattering coefficients times the thickness are necessary, which can be achieved most commonly by dilution of the sample or using thin slabs or cylinders. For emulsions a dilution can change the droplet size in the sample and the measurement through a thin slab or cylinder can cause hygienic difficulties in a milk process line. A dilution of the sample or a bypass through a thin slab in the process line is not necessary for the presented method, which is another great advantage of the lateral transmission setup.

References

[1] RAJ Groenhuis, Hedzer A Ferwerda, and JJ Ten Bosch. Scattering and absorption of turbid materials determined from reflection measurements. 1: Theory. *Applied optics*, 22(16): 2456–2462, 1983.

[2] RAJ Groenhuis, JJ Ten Bosch, and Hedzer A Ferwerda. Scattering and absorption of turbid materials determined from reflection measurements. 2: Measuring method and calibration. *Applied optics*, 22(16):2463–2467, 1983.

[3] Michael S Patterson, Ephraim Schwartz, and Brian C Wilson. Quantitative reflectance spectrophotometry for the noninvasive measurement of photosensitizer concentration in tissue during photodynamic therapy. In *Proc. SPIE*, volume 1065, pages 115–122, 1989.

[4] Brian C Wilson and Steven L Jacques. Optical reflectance and transmittance of tissues: principles and applications. *IEEE Journal of Quantum Electronics*, 26(12):2186–2199, 1990.

[5] Stephen T Flock, Steven L Jacques, Brian C Wilson, Willem M Star, and Martin JC van Gemert. Optical properties of intralipid: a phantom medium for light propagation studies. *Lasers in surgery and medicine*, 12(5):510–519, 1992.

[6] John W Pickering, Christian JM Moes, HJCM Sterenborg, Scott A Prahl, and Martin JC Van Gemert. Two integrating spheres with an intervening scattering sample. *JOSA A*, 9(4): 621–631, 1992.

[7] John W Pickering, Scott A Prahl, Niek Van Wieringen, Johan F Beek, Henricus JCM Sterenborg, and Martin JC Van Gemert. Double-integrating-sphere system for measuring

the optical properties of tissue. *Applied optics*, 32(4):399–410, 1993.

[8] Scott A Prahl, Martin JC van Gemert, and Ashley J Welch. Determining the optical properties of turbid media by using the adding–doubling method. *Applied optics*, 32(4):559–568, 1993.

[9] Michael S Patterson, Britton Chance, and Brian C Wilson. Time resolved reflectance and transmittance for the noninvasive measurement of tissue optical properties. *Applied optics*, 28(12):2331–2336, 1989.

[10] Antonio Pifferi, Alessandro Torricelli, Paola Taroni, Daniela Comelli, Andrea Bassi, and Rinaldo Cubeddu. Fully automated time domain spectrometer for the absorption and scattering characterization of diffusive media. *Review of scientific instruments*, 78(5):053103, 2007.

[11] Michael S Patterson, J David Moulton, Brian C Wilson, Klaus W Berndt, and Joseph R Lakowicz. Frequency-domain reflectance for the determination of the scattering and absorption properties of tissue. *Applied optics*, 30(31):4474–4476, 1991.

[12] Bruce J Tromberg, Olivier Coquoz, Joshua B Fishkin, Tuan Pham, Eric R Anderson, John Butler, Mitchell Cahn, Jeffrey D Gross, Vasan Venugopalan, and David Pham. Non-invasive measurements of breast tissue optical properties using frequency-domain photon migration. *Philosophical Transactions of the Royal Society of London B: Biological Sciences*, 352(1354):661–668, 1997.

[13] Joshua B Fishkin, Olivier Coquoz, Eric R Anderson, Matthew Brenner, and Bruce J Tromberg. Frequency-domain photon migration measurements of normal and malignant tissue optical properties in a human subject. *Applied optics*, 36(1):10–20, 1997.

[14] Oliver Reich, Hans-Gerd Löhmannsröben, and Frank Schael. Optical sensing with photon density waves: investigation of model media. *Physical Chemistry Chemical Physics*, 5(23):5182–5187, 2003.

[15] S. Chandrasekhar. *Radiative Transfer*. Dover Publications Inc., 1960.

[16] Josip P. Kratohvil and Colin Smart. Calibration of light-scattering instruments. iii. absolute angular intensity measurements on mie scatterers. *J. Colloid Sci.*, 20(8):875–892, 1965.

[17] Edouard Berrocal, David L Sedarsky, Megan E Paciaroni, Igor V Meglinski, and Mark A Linne. Laser light scattering in turbid media part i: Experimental and simulated results for the spatial intensity distribution. *Optics express*, 15(17):10649–10665, 2007.

[18] Fabrice Vaudelle, Jean-Pierre LHuillier, and Mohamed Lamine Askoura. Light source distribution and scattering phase function influence light transport in diffuse multi-layered media. *Optics Communications*, 392:268–281, 2017.

[19] S. Stocker, F. Foschum, P. Krauter, F. Bergmann, A. Hohmann, C. Scalfi Happ, and A. Kienle. Broadband optical properties of milk. *Appl. Spectrosc.*, 71(5):951–962, May 2017. doi: 10.1177/0003702816666289.

[20] Hiroyuki Mima and Nobuyuki Kitamori. Stability and flocculation of oil droplet in dilute emulsions. *Journal of pharmaceutical sciences*, 55(1):44–48, 1966.

[21] E Shotton and SS Davis. The use of the coulter counter for the particle size analysis of some emulsion systems. *Journal of Pharmacy and Pharmacology*, 20(6):430–438, 1968.

[22] E Shotton and SS Davis. A note on the stability of emulsions at high dilution. *Journal of Pharmacy and Pharmacology*, 20(11):825–829, 1968.

[23] Douglas G. Dalgleish. Adsorption of protein and the stability of emulsions. *Trends Food Sci. Technol.*, 8(1):1–6, Jan 1997.

[24] C. Tribastone and W. Peck. *Designing plastic optics: New applications emerging for optical glass substitutes*. Laurin Publishing, 1998.

[25] Louis G. Henyey and Jesse Leonard Greenstein. Diffuse radiation in the galaxy. *Astrophys. J.*, 93(1):70–83, Jan 1941. doi: 10.1086/144246.

[26] P. Krauter, S. Nothelfer, N. Bodenschatz, E. Simon, S. Stocker, F. Foschum, and A. Kienle. Optical phantoms with adjustable subdiffusive scattering parameters. *J. Biomed. Opt.*, 20(10):105008–105008, 2015.

[27] Lamont R Poole, Demetrius D Venable, and Janet W Campbell. Semianalytic monte carlo radiative transfer model for oceanographic lidar systems. *Applied optics*, 20(20):3653–3656, 1981.

[28] Alwin Kienle, Raimund Hibst, and Rudolf W Steiner. Use of a neural network and monte carlo simulations to determine the optical coefficients with spatially resolved transmittance measurements. In *Society of Photo-Optical Instrumentation Engineers (SPIE) Conference Series*, volume 2134, pages 364–371, 1994.

[29] Florian Foschum. *Bestimmung der optischen Eigenschaften trüber Medien mittels nichtinvasiver Remissionsmessungen*. PhD thesis, Universität Ulm, 2012.

[30] Nico Bodenschatz, Philipp Krauter, André Liemert, and Alwin Kienle. Quantifying phase function influence in subdiffusively backscattered light. *Journal of biomedical optics*, 21(3):035002–035002, 2016.

[31] B. Aernouts, E. Polshin, J. Lammertyn, and W. Saeys. Visible and near-infrared spectroscopic analysis of raw milk for cow health monitoring: Reflectance or transmittance? *J. Dairy Sci.*, 94(11):5315–5329, 2011.

[32] Salomé Vargas Ruiz, Roland Hass, and Oliver Reich. Optical monitoring of milk fat phase transition within homogenized fresh milk by photon density wave spectroscopy. *International dairy journal*, 26(2):120–126, 2012.

[33] B. Aernouts, R. Van Beers, R. Watté, T. Huybrechts, J. Lammertyn, and W. Saeys. Visible and near-infrared bulk optical properties of raw milk. *J. Dairy Sci.*, 98(10):6727–6738, 2015.

[34] O. H. A. Abildgaard, F. Kamran, A. B. Dahl, J. L. Skytte, F. D. Nielsen, C. L. Thomsen, P. E. Andersen, R.s Larsen, and J. R. Frisvad. Non-invasive assessment of dairy products using spatially resolved diffuse reflectance spectroscopy. *Appl. Spectrosc.*, 69(9):1096–1105, 2015.

[35] O. H. A. Abildgaard, J. R. Frisvad, V. Falster, A. Parker, N. J. Christensen, A. B. Dahl, and R. Larsen. Noninvasive particle sizing using camera-based diffuse reflectance spectroscopy. *Applied optics*, 55(14):3840–3846, 2016.

[36] F. Kamran and P. E. Andersen. Sensitivity analysis for oblique incidence reflectometry using monte carlo simulations. *Appl. Opt.*, 54(23):7099–7105, 2015.

[37] A. Bogomolov, S. Dietrich, B. Boldrini, and R. W. Kessler. Quantitative determination of fat and total protein in milk based on visible light scatter. *Food Chemistry*, 134(1):412–418, 2012.

[38] A. Bogomolov and A. Melenteva. Scatter-based quantitative spectroscopic analysis of milk fat and total protein in the region 400–1100nm in the presence of fat globule size variability. *Chemometrics and Intelligent Laboratory Systems*, 126:129–139, 2013.